J. Fluid Mech. (2008), *vol.* 607, *pp.* 167–197. © 2008 Cambridge University Press
doi:10.1017/S0022112008001973 Printed in the United Kingdom

Numerical and theoretical study of the shock stand-off distance in non-equilibrium flows

N. BELOUAGGADIA[1], H. OLIVIER[2] AND R. BRUN[1]

[1]Université de Provence, Marseille, France

[2]RWTH Aachen University, Aachen, Germany

(Received 24 July 2007 and in revised form 13 March 2008)

A theoretical model based on a quasi-one-dimensional formulation is developed which allows determination of the shock stand-off distance at the stagnation point of blunt bodies in hypersonic non-equilibrium flows. Despite the simple ideal dissociating gas model implemented in the theoretical approach, it gives insight into the main physics governing the shock stand-off problem. More detailed and precise data are obtained by a numerical simulation where vibrational and chemical relaxation processes as well as their interactions are taken into account. The physical modelling of these processes is based on a kinetic approach and on a generalized Chapman–Enskog method of solving the Boltzmann equation. Explicit formulae for rate constants and vibrational energy consumption are derived and incorporated into the general conservation equations. Good agreement between theoretical, numerical and experimental results is achieved which ensures a reliable and mutual validation of the different methods.

1. Introduction

A spacecraft entering the atmosphere at orbital speed encounters extremely high gas temperatures behind the bow shock and especially in the stagnation region. These high temperatures of the order of several thousand degrees are due to the conversion of kinetic flow energy into thermal energy by shock compression leading to strong molecular collisions. According to the arguments of statistical mechanics, some of these collisions lead to the excitation of higher modes of the vibrational energy and to a variety of chemical reactions where the constituents differ for different gas compositions. Dominant for the stagnation flow field for typical re-entry conditions are dissociation reactions of the molecules. Depending on the reaction and excitation rates, these thermal and chemical processes may take place in nearly frozen, non-equilibrium or nearly equilibrium conditions.

One of the important parameters characterizing the blunt-body flow field in the stagnation region is the shock stand-off distance. This parameter is often employed for validation purposes of numerical methods as well as for non-reactive and reactive gases. Since for high Mach number flows the shock is very close to the body, i.e. the stand-off distance is small with respect to a characteristic body length, its experimental determination is difficult and relatively large errors have to be accepted. Therefore, any reliable data of the stand-off distance determined by theoretical and/or numerical solutions is of great significance in the discussion of this physical phenomenon. In general, theoretical methods do not provide a solution of the whole flow field, but often enable recognition and to study of the influence of the main physical parameters of the problem considered. On the other hand, numerical solutions provide detailed

knowledge of the whole flow field and therefore of all flow parameters for the particular free-stream and boundary conditions chosen. Therefore, in this paper both numerical simulations and a theoretical approach are used to allow a much deeper understanding of the physical phenomena relevant for the problem of the shock stand-off distance in reactive flows.

For perfect gas flow, many theoretical and numerical solutions have been published. Based on the well-known constant density concept, Hayes & Probstein (1959) gave solutions for the cylinder and flow around a sphere. Of course, for reacting flows the reactions taking place behind the bow shock alter the density field significantly, and so the assumption of a constant density in the shock layer is not well suited to this flow regime. A variety of inverse methods have been applied to the problem of a flow with a detached shock at a blunt nose. For the inverse problem the shape of the shock is given and the shape of the body and the details of the flow field in the shock layer are determined. The main idea is that, if the shape of the detached shock is prescribed, the values of the flow variables just behind the shock can be found easily from oblique shock relations. This also holds for the gradients of flow parameters tangent to the shock. Based on these boundary values, the flow field between shock and body is represented by appropriate power series expansion, as was done e.g. by Lin & Shen (1951). Another approach has been given by Zlotnick & Newman (1957) who developed an inverse method by rearranging the conservation equations in shock-oriented orthogonal curvilinear coordinates such that they could be successively solved for the values of the derivatives normal to the shock. Again, the inflow is given by the shock conditions. The same principle has been applied by Van Dyke (1958) whose solution for the stand-off distance in perfect gas conditions is still used today as reference data. The determination of the subsonic part of the flow field for the inverse formulation is governed by an elliptic partial differential equation and is carried out as an initial value problem with Cauchy data, i.e. the value of a function, and of its normal derivative specified along the shock wave. Though from a mathematical point of view a Cauchy problem for an elliptic differential equation is ill-posed resulting in general in numerical problems, the accuracy achieved with these methods is very high. During the computational procedure, the shock shape is successively changed until the desired body shape is achieved. The main idea of the theoretical approach described in § 2 is similar to the concept of the inverse problem.

For non-equilibrium flow, the inverse method was first applied by Lick (1960) and has been extended for more realistic chemical kinetics of high temperature air by Hall, Eschenroeder & Marrone (1962). Hornung (1972) applied the numerical methods of Freeman (1958) based on the ideal dissociating gas model and of Garr & Marrone (1957) including vibrational relaxation and the kinetics of a mixture of gases to study the non-equilibrium flow over spheres and cylinders. In that paper Hornung showed that the shock stand-off distance also depends on a reaction rate parameter which describes the gradient of the dissociation level immediately behind the shock. For frozen flow, i.e. low reaction rate parameters, as expected, the stand-off distance is larger than for equilibrium flow, characterized by a high reaction rate parameter. Wen & Hornung (1995) extended these previous results by an approximate theory which relates the dimensionless shock stand-off distance to a modified reaction rate parameter valid for more general gas mixtures. It is important to note that based on this theoretical approach assuming linear density profiles between shock and body, Wen & Hornung showed that the shock stand-off distance not only depends on the reaction rate parameter but also on the density ratio between shock and body as

additional parameter. For frozen and equilibrium flow this has also been found by Olivier (2000) who gave an analytical solution for the stand-off distance based on the solution of the continuity equation in a quasi-one-dimensional formulation.

In the first part of this paper, this theoretical solution is extended to the non-equilibrium flow regime and compared with numerical results. As expected, the non-equilibrium processes increase the complexity of the conservation equations so that even for the quasi-one-dimensional approach an analytical solution is no longer possible. However, the method described is still very simple and yields a thorough understanding of the relevant physical phenomena.

The second part of the paper deals with the numerical determination of the hypersonic flow field around blunt bodies. This is based on two essential features. The first consists of using a realistic physical model taking correctly into account the physical phenomena inherent in high-enthalpy flows such as vibrational excitation, dissociation and various reactions having characteristic times similar to the reference flow time. The modelling of these phenomena and of the associated non-equilibrium flows has been the subject of many studies, so that the main characteristics of these flows are now well-known. Accordingly, much data exists for the translation/vibration (TV) and the vibration/vibration (VV) transition probabilities and corresponding relaxation times as well as the reaction rate constants and also the coupling between vibrational excitation and chemical reactions. Very few complete analyses of non-equilibrium flows are available however. That has motived the first and third author to develop such a systematic study for pure gases as well as for mixtures. This analysis is based on a kinetic approach and on the Chapman–Enskog method for solving the Boltzmann equation, taking into account a hierarchy of characteristic times of various processes. Because of the variable time scales of these processes, the Chapman-Enskog procedure is non-unique and depends on the physical conditions. Thus, a generalized Chapman-Enskog method is developed, allowing the description of general cases of vibrational and chemical non-equilibrium. The only assumptions remaining are that the characteristic time of vibrational relaxation remains shorter than or equal to the chemical time and that regions of steep gradients are excluded from consideration. Explicit formulae for rate constants and vibrational energy consumption are derived and incorporated into the general conservation equations for species and vibrational energy, thus closing the Navier–Stokes set of equations for non-equilibrium flow. The numerical method used to solve this set of equations is completely implicit, second-order accurate in time and space, using a Gauss–Seidel line relaxation scheme. A time-developing solution is obtained up to the required steady state. Finally, the computed values of the shock stand-off distance over hemispherical bodies are compared with available experimental data and with values from the theory presented in the first part of the paper.

A comparison of experimental, numerical and theoretical data shows that they are consistent. Furthermore, they complement each other and allow a thorough discussion of the important physical phenomena relevant for the shock stand-off distance in non-equilibrium flow conditions.

2. Theoretical modelling of the shock stand-off distance in non-equilibrium flow

Because some relations and definitions reported by Wen & Hornung (1995) and Olivier (2000) are essential for the understanding of the following, the most important ones are briefly summarized.

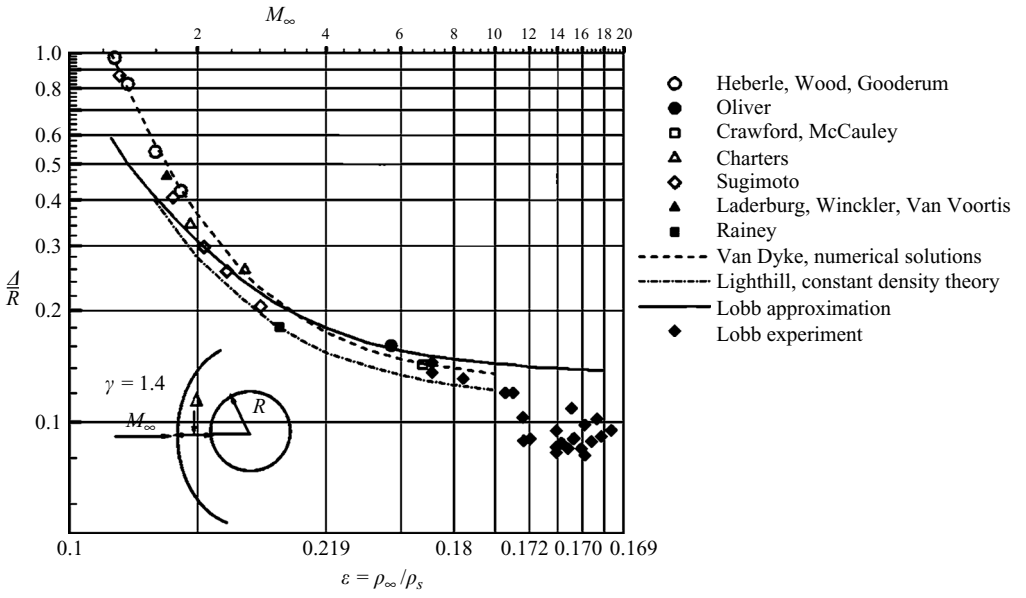

FIGURE 1. Comparison of different experimental and theoretical data for the shock stand-off distance on a sphere. The symbols correspond to experimental data used by van Dyke (1958) to check his numerical solution, with the exception of the diamond, which is from Lobb (1964).

The numerical solution of Van Dyke (1958) for a non-reactive gas has been approximated by Lobb (1964) who gave the well-known relation

$$\frac{\Delta_{fr}}{D} = 0.41\,\frac{\rho_\infty}{\rho_s} \tag{2.1}$$

with Δ the stand-off distance, D the sphere diameter and ρ_s the density immediately behind the shock. Figure 1 shows a comparison of Van Dyke's numerical solution, the approximation given by Lobb (2.1) and experimental data used by Van Dyke to check his solution. Also, the experimental results of Lobb are added; he measured the shock stand-off distance on spheres in a two-stage light gas gun for the high Mach number range. It is seen that the numerical solution of Van Dyke fits very well with the experimental data for the low supersonic Mach number range up to about 8. This is not surprising, because the experimental data referenced by Van Dyke as well as Van Dyke's numerical solution cover the range of perfect gas behaviour. It is also clear that the approximation given by Lobb fits well to the data for a Mach number range from 2 to 8 but not for higher Mach number or flight velocity range. That is also not surprising, because as has been shown by Wen & Hornung (1995), the simple relation (2.1) given by Lobb is not suited to cover high-temperature effects. These become evident in the experimental data of Lobb for the high Mach number range. As expected, these effects lead to a reduction of the shock stand-off distance compared to the perfect gas data. Newer experiments show that quantitatively the data given by Lobb (1964) might have been influenced by some experimental shortcomings resulting in an error of a few percent in the stand-off distance. However, the qualitative behaviour is well described. The data presented in figure 1 as well as more recently published experimental and numerical data, show that the evaluation of the shock stand-off distance in reacting flows needs more comprehensive models and correlations than used in the past.

Concerning the modelling, Wen & Hornung (1995) extended previous results of Hornung (1972) by an approximated theoretical approach which relates the dimensionless shock stand-off distance

$$\tilde{\Delta} = \frac{\Delta}{D}\,\frac{\rho_s}{\rho_\infty} \tag{2.2}$$

to a reaction rate parameter of the form

$$\tilde{\Omega}_s = \left(\frac{\mathrm{d}\rho}{\mathrm{d}t}\right)_s \frac{D}{\rho_s u_\infty}, \tag{2.3}$$

where the index s indicates conditions immediately behind the shock. This approximate theory assumes piecewise-linear density profiles between the shock and the body. From the specific density profile an average density value ρ_{av} is determined which is related to the shock stand-off distance by the ansatz (Wen & Hornung 1995)

$$\tilde{\Delta} = 0.41\,\frac{\rho_s}{\rho_{av}}. \tag{2.4}$$

In this approach the influence of the reactive flow between shock and body on the stand-off distance is taken into account by the averaged value of the density profile. The solution of the corresponding equation for the shock stand-off distance shows its dependence not only on the reaction rate parameter but also on the density ratio between shock and body. This influence becomes dominant for flow conditions in the shock layer which are close to equilibrium.

The aim of the theoretical method presented in this paper is to determine the shock stand-off distance for a sphere and cylinder for the whole non-equilibrium flow regime, ranging from frozen to equilibrium flow, and so this method is based on the solution of the conservation equations which are simplified in a suitable manner. Compared to the analytical solution given by Olivier (2000) for frozen and equilibrium flow, some previous restrictions can be removed and the formulation presented is more accurate and valid in a wider range.

The continuity and impulse equations in the circumferential direction for cylindrical coordinates are given by

$$\frac{\partial}{\partial r}[\rho v r(r\sin\phi)^\eta] + \frac{\partial}{\partial \phi}[\rho u (r\sin\phi)^\eta] = 0 \tag{2.5}$$

and

$$\rho v\,\frac{\partial u}{\partial r} + \frac{\rho u}{r}\left(\frac{\partial u}{\partial \phi} + v\right) + \frac{1}{r}\frac{\partial p}{\partial \phi} = 0, \tag{2.6}$$

where $\eta = 0$ for a plane flow and $\eta = 1$ for a flow of rotational symmetry. These equations are non-dimensionalized using

$$\left.\begin{aligned} &\bar{p} = \frac{p}{p_b}, \quad \bar{\rho} = \frac{\rho}{\rho_b}, \quad \bar{u} = \frac{u}{u_{ref}}, \quad \bar{v} = \frac{v}{u_{ref}}, \quad \bar{h} = \frac{h}{h_{tot}}, \\ &\bar{T} = \frac{T}{T_{ref}}, \quad \bar{\Theta}_d = \frac{\Theta_d}{T_{ref}}, \quad \bar{r} = \frac{2r}{D}, \quad \bar{\Delta} = \frac{2\Delta}{D} \end{aligned}\right\} \tag{2.7}$$

with

$$h_{tot} = R_{A_2}\,T_{ref} = \frac{u_{ref}^2}{2} \approx \frac{u_\infty^2}{2}.$$

An inviscid flow is considered for this theoretical model, i.e. the results are valid for flow conditions where in particular the boundary layer around the body has

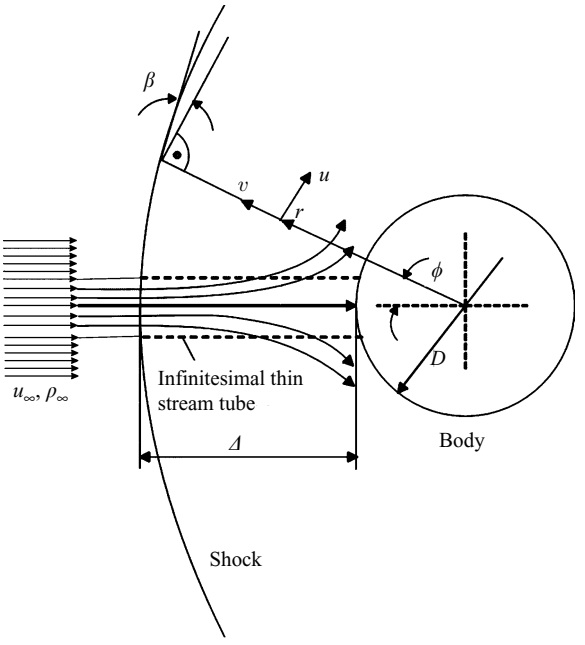

FIGURE 2. Coordinate system of the streamtube model.

no significant influence on the stand-off distance. This is usually the case for the hypersonic flow regime of interest for which non-equilibrium effects are important.

As is usual for hypersonic free-stream conditions, the contribution of the static enthalpy to the total enthalpy is neglected. A normalized coordinate $r^* = (\bar{r} - 1)/\bar{\Delta}$ is introduced which varies between 0 at the body and 1 at the shock. In the following, the index b denotes conditions at the body surface and s values immediately behind the shock. It is assumed that the flow across the shock is frozen. For the solution of the conservation equations a quasi-one-dimensional approach is utilized which describes the flow in the close vicinity of the stagnation streamline. In other words, along the stagnation streamline a streamtube of infinitely small cross-section is considered (see figure 2). It is the continuity condition for this streamtube which from a physical point of view yields the shock stand-off distance.

After differentiating and introducing the following approximations and conditions usual for the flow in the vicinity of the stagnation streamline:

$$\sin\phi \approx \phi, \quad \bar{u} = \phi \frac{\partial \bar{u}}{\partial \phi}, \quad \frac{\partial \bar{\rho}}{\partial \phi} = 0, \tag{2.8}$$

the non-dimensionalized continuity equation is given by

$$\frac{\bar{v}}{\bar{\rho}} \frac{\partial \bar{\rho}}{\partial r^*} + \frac{\partial \bar{v}}{\partial r^*} + (\eta + 1) \frac{\bar{\Delta}\bar{v}}{1 + \bar{\Delta} r^*} + (\eta + 1) \frac{\bar{\Delta}}{1 + \bar{\Delta} r^*} \frac{\partial \bar{u}}{\partial \phi} = 0, \tag{2.9}$$

where in the following $\eta = 0$ describes the flow across a cylinder and $\eta = 1$ the flow over a sphere. The non-dimensionalized impulse equation follows from (2.6) and the approximations given in (2.8),

$$\bar{\rho}\bar{v} \frac{\partial}{\partial r^*} \left(\frac{\partial \bar{u}}{\partial \phi} \right) + \frac{\bar{\Delta}}{1 + \bar{\Delta} r^*} \bar{\rho} \frac{\partial \bar{u}}{\partial \phi} \left(\frac{\partial \bar{u}}{\partial \phi} + \bar{v} \right) + \frac{2\bar{\Delta}}{1 + \bar{\Delta} r^*} \frac{p_b}{\rho_b h_{tot}} \frac{1}{\phi} \frac{\partial \bar{p}}{\partial \phi} = 0, \tag{2.10}$$

where for the stagnation streamline the pressure gradient $\partial \bar{p}/\partial \phi$ is zero, but not the term $(1/\phi)\,\partial \bar{p}/\partial \phi$ which is a measure of the second derivative of the pressure distribution in the circumferential direction. For simplicity, in this theoretical model an ideal dissociating gas according to Freeman (1958) has been assumed, i.e. the degree of dissociation α is given by

$$\frac{\mathrm{d}\alpha}{\mathrm{d}t} = C T^{\nu} \rho \left[(1-\alpha)\, \mathrm{e}^{-\Theta_d/T} - \frac{\rho}{\rho_d}\, \alpha^2 \right], \tag{2.11}$$

where the first term in the brackets describes the dissociation and the second one the recombination reaction. In non-dimensional form this equation is

$$\frac{\mathrm{d}\alpha}{\mathrm{d}r^*} = \Lambda\, \frac{\rho_b}{\rho_s}\, \frac{\rho_s}{\rho_\infty}\, \frac{\bar{\rho}\bar{\Delta}}{|\bar{v}|}\, \bar{T}^{\nu} \left[(1-\alpha)\, \mathrm{e}^{-\bar{\Theta}_d/\bar{T}} - \bar{\rho}\, \frac{\rho_b}{\rho_s}\, \frac{\rho_s}{\rho_d}\, \alpha^2 \right], \tag{2.12}$$

where the constant Λ is given by

$$\Lambda = C T_{ref}^{\nu}\, \frac{\rho_\infty D/2}{u_{ref}}, . \tag{2.13}$$

Physically, this represents a kind of reaction rate parameter which determines how fast the reaction rate changes along the stagnation streamline. The parameter $\bar{\Theta}_d$ in (2.12),

$$\bar{\Theta}_d = \frac{E_{diss}\, R_{A_2}/K}{u_{ref}^2/2}, \tag{2.14}$$

represents the ratio of the dissociation energy of one molecule A_2 to its kinetic energy in the free stream. It will be seen that this dissociation energy parameter has a significant influence on the non-equilibrium flow between shock and body. To close the set of equations, an equation of state and the energy conservation equation are necessary. For the ideal dissociating gas the non-dimensionalized equation of state is given by

$$\bar{\rho} = \frac{\bar{p}}{(1+\alpha)\,\bar{T}}\, \frac{p_b}{\rho_b h_{tot}}, \tag{2.15}$$

where the factor including the reference conditions follows from the conditions at the stagnation point

$$\frac{p_b}{\rho_b h_{tot}} = (1+\alpha_b)\, \bar{T}_b. \tag{2.16}$$

The non-dimensionalized temperature at the stagnation point can be found from the enthalpy of the ideal dissociating gas

$$h = (4+\alpha)\, R_{A_2} T + \alpha\, R_{A_2} \Theta_d, \tag{2.17}$$

which for the stagnation point leads to

$$\bar{T}_b = \frac{1-\alpha_b \bar{\Theta}_d}{4+\alpha_b}. \tag{2.18}$$

The temperature along the stagnation streamline is determined by the conservation of the total enthalpy

$$\bar{T} = \frac{1-\alpha\, \bar{\Theta}_d - \bar{v}^2}{4+\alpha}, \tag{2.19}$$

so that the density follows from (2.15):

$$\bar{\rho} = \frac{4+\alpha}{1+\alpha}\,\frac{1+\alpha_b}{4+\alpha_b}\,\frac{(1-\alpha_b\,\bar{\Theta}_d)\bar{p}}{1-\alpha\,\bar{\Theta}_d-\bar{v}^2}. \tag{2.20}$$

The system of the five equations (2.9), (2.10), (2.12), (2.19) and (2.20) describing the quasi one-dimensional model of the stagnation point flow contains seven unknowns $\bar{\rho}$, $\bar{p}$, $\bar{T}$, α, $\bar{v}$, $\partial\bar{u}/\partial\phi$ and $(1/\phi)\,\partial\bar{p}/\partial\phi$. The shock stand-off distance $\bar{\Delta}$ follows from the solution of this set of equations with the boundary condition that the velocity $\bar{v}$ must be zero at the stagnation point. Therefore, in order to solve the set of equations, two parameters have to be prescribed by introducing suitable approximations. On one hand, the need for this results from the quasi one-dimensional approach. On the other hand, this model avoids the solution of a two-dimensional flow problem which from an analytical and/or numerical point of view is much more complicated than for the one-dimensional case. But, as is well known, the accuracy achieved by a multi-dimensional approach strongly depends on the method of solution, numerical issues, etc. For certain phenomena the multi-dimensional approach is not necessarily more accurate than a one-dimensional formulation, particularly if the one-dimensional model is adapted to the phenomenon of interest and necessary assumptions are introduced in a way that their influence on the solution is as weak as possible. The smallest variations along the stagnation streamline show the non-dimensionalized pressure $\bar{p}$ and the derivative term in $(1/\phi)\,\partial\bar{p}/\partial\phi$. The pressure along the stagnation streamline typically changes not more than 5 % to 10 %. Therefore, in this flow model as first approximation the pressure is set to be constant. As shown in the following, the value of the term $(1/\phi)\,\partial\bar{p}/\partial\phi$ in the tangential momentum equation changes between the stagnation point and shock by a factor of $2/(\gamma+1)[1-\partial\beta/\partial\phi]$, where γ is the ratio of the specific heats for frozen flow across the shock. For a gas such as air, the variation of this term amounts to 25 % which is much less than the variation of the other variables. Therefore, as second approximation the variation of this parameter between shock and body is assumed to be linear. Knowing the values of this parameter at the shock and at the body and also the boundary conditions of the other variables, the set of equations given above can be solved to finally determine the shock stand-off distance.

The determination of the gradient term $((1/\phi)\,\partial\bar{p}/\partial\phi)_s$ as one boundary condition is based on the oblique shock relation

$$\frac{p_s}{p_\infty} = 1 + \frac{2\gamma}{\gamma+1}\left(M_\infty^2\sin^2\sigma - 1\right), \tag{2.21}$$

where σ is the shock angle and M_∞ the free-stream Mach number. Since the flow is assumed to be frozen across the shock, this relation holds also for reactive flow conditions. Replacing the shock angle σ by $\sigma = \beta - \phi + \pi/2$ (see figure 2) leads to

$$\left(\frac{\partial p}{\partial\phi}\right)_s = -\frac{4\gamma}{\gamma+1}\,M_\infty^2 p_\infty(\beta-\phi)\left(\frac{\partial\beta}{\partial\phi}-1\right) \tag{2.22}$$

which finally gives with (2.7) and $\beta = 0^\circ$ for the stagnation streamline

$$\left(\frac{1}{\phi}\,\frac{\partial\bar{p}}{\partial\phi}\right)_s = -\frac{8}{\gamma+1}\left[1-\frac{\partial\beta}{\partial\phi}\right]\frac{\rho_\infty}{\rho_s}\,\frac{\rho_s}{\rho_b}\,\frac{\rho_b h_{tot}}{p_b}. \tag{2.23}$$

The boundary condition of the pressure gradient term at the stagnation point is determined by the assumption of a Newtonian pressure distribution along the body

which represents an approximation of sufficient high accuracy for hypersonic flow conditions, i.e.

$$p - p_\infty = 2\, q_\infty \cos^2 \phi. \tag{2.24}$$

Following the same procedure as for (2.23) and with $p \gg p_\infty$ it follows that

$$\left(\frac{1}{\phi}\frac{\partial \bar{p}}{\partial \phi}\right)_b = -4\,\frac{\rho_\infty}{\rho_s}\,\frac{\rho_s}{\rho_b}\,\frac{\rho_b h_{tot}}{p_b}. \tag{2.25}$$

Knowing the two values given by (2.23) and (2.25) which only differ by about 25 %, the pressure gradient term in (2.10) is approximated by a linear distribution between shock and body as stated above. Additionally to the pressure gradient term, the tangential velocity gradient just behind the shock and at the stagnation point have to be prescribed as a boundary condition. At the shock the tangential velocity gradient follows from the tangential velocity component which is conserved across the shock,

$$u = u_\infty \sin(\phi - \beta). \tag{2.26}$$

For the stagnation streamline with $\phi = \beta = 0°$ this leads to

$$\left(\frac{\partial \bar{u}}{\partial \phi}\right)_s = 1 - \left(\frac{\partial \beta}{\partial \phi}\right)_s. \tag{2.27}$$

The tangential velocity gradient at the stagnation point follows from the impulse equation (2.10) for $\bar{\rho} = 1$ and $\bar{v} = 0$:

$$\left(\frac{\partial \bar{u}}{\partial \phi}\right)_b = \sqrt{-\frac{1}{2}\,\frac{p_b}{\rho_b h_{tot}}\left(\frac{1}{\phi}\frac{\partial \bar{p}}{\partial \phi}\right)_b}. \tag{2.28}$$

The tangential pressure gradient in (2.28) is given by (2.25) which finally leads to

$$\left(\frac{\partial \bar{u}}{\partial \phi}\right)_b = \sqrt{2\,\frac{\rho_\infty}{\rho_s}\,\frac{\rho_s}{\rho_b}}. \tag{2.29}$$

It is not surprising that the tangential velocity gradient inversely depends on the density at the stagnation point, because from mass conservation for the stagnation line streamtube it follows that the higher the density the lower the tangential velocity, i.e. the lower the tangential velocity gradient. The mass flux leaving the stagnation region is determined by the density and the tangential velocity component.

As a further boundary condition the degree of dissociation at the stagnation point α_b has to be determined. For the flow model considered, the flow at the stagnation point is in equilibrium. This holds regardless of the magnitude of the reaction rate parameter since the velocity at the stagnation point is zero and therefore, the residence time approaches infinity. In this case, the term in the brackets of (2.12) is equal to zero from which the temperature at the stagnation point can be deduced:

$$\bar{T}_b = \bar{\Theta}_d \ln^{-1}\left(\frac{\rho_d}{\rho_s}\,\frac{\rho_s}{\rho_b}\,\frac{1-\alpha_b}{\alpha_b^2}\right). \tag{2.30}$$

From the conservation of the total enthalpy, a second equation follows for the temperature (see (2.18)):

$$\bar{T}_b = \frac{1 - \alpha_b \bar{\Theta}_d}{4 + \alpha_b}, \tag{2.31}$$

which gives together with (2.30) a relation between the degree of dissociation at the body and the non-dimensional dissociation energy:

$$\bar{\Theta}_d = \ln\left(\frac{\rho_d}{\rho_s}\frac{\rho_s}{\rho_b}\frac{1-\alpha_b}{\alpha_b^2}\right)\left[4+\alpha_b+\alpha_b\ln\left(\frac{\rho_d}{\rho_s}\frac{\rho_s}{\rho_b}\frac{1-\alpha_b}{\alpha_b^2}\right)\right]^{-1}. \tag{2.32}$$

From (2.20) the density ratio between shock and body is given by

$$\frac{\rho_s}{\rho_b} = \frac{4(1-\alpha_b\bar{\Theta}_d)(1+\alpha_b)}{4+\alpha_b}, \tag{2.33}$$

where it has been assumed for simplicity that there is no free-stream dissociation, $\bar{p}$ is equal to 1 as stated above and $\bar{v}^2 \ll 1$. The validity of $\bar{p}=1$ and $\bar{v}^2 \ll 1$ has been proven by numerous numerical and theoretical solutions for a hypersonic stagnating flow around blunt bodies. As expected, equations (2.32) and (2.33) show that the density ratio between shock and body, the degree of dissociation at the body α_b, and for a given gas the total enthalpy of the flow occurring in the denominator of the non-dimensional dissociation energy $\bar{\Theta}_d$, are not independent. Equations (2.32) and (2.33) are solved by prescribing one of the three parameters, where in this case the density ratio between shock and body has been chosen as free parameter in accordance with the model of Wen & Hornung (1995). In this case, the degree of dissociation α_b and the non-dimensional dissociation energy follow from (2.32) and (2.33). The evaluation of these two equations show that as expected the establishment of a large density ratio ρ_b/ρ_s between body and shock requires a high total enthalpy of the flow, corresponding to a small non-dimensional dissociation energy $\bar{\Theta}_d$. For a given gas the parameter $\bar{\Theta}_d$ describes the total enthalpy of the flow, and so it yields the relation between the density ratio ρ_s/ρ_b used as a parameter in the theory and the total enthalpy used as a parameter for the experimental data as in the following. With increasing density ratio ρ_b/ρ_s, the rate of dissociation α_b at the stagnation point also increases. It is interesting to note that for a given value of the parameter ρ_d/ρ_s, such as $\rho_d/\rho_s = 10^7$ as proposed by Lighthill, from equations (2.32) and (2.33) a solution follows only for density ratios ρ_b/ρ_s larger than 0.5. This means that for a particular chemical model the range of density variation between shock and body is limited.

It is quite often stated that recombination reactions take place in a very narrow region close to the body surface and therefore are of no significant importance for the computation of global flow field phenomena such as the stand-off distance. The ideal dissociating gas model nicely shows that this statement has to be handled with care. This is also the case for more complicated chemical models. Neglecting the recombination reaction in (2.12) means that at the stagnation point the first term in the brackets has to go to zero which is only possible for $\alpha_b = 1$, i.e. complete dissociation takes place at the stagnation point. But in this case $\bar{\Theta}_d \leqslant 1$ or $T_{ref} \geqslant \Theta_d$ which follows from (2.18). The characteristic dissociation temperature Θ_d for oxygen is 59 500 K, and for nitrogen is 113 000 K. This makes clear that for a gas model which does not allow recombination reactions, the assumption of an equilibrium flow at the stagnation point requires total flow enthalpies $h_{tot} = R_{A_2}T_{ref}$ magnitudes with unreasonable. This is based on the requirement of complete dissociation at the stagnation point. Corresponding to this, the temperature at the stagnation point is also much higher than for the case with recombination reactions. In this case, the erroneous boundary conditions at the stagnation point may not only influence the flow field close to the surface but also further upstream in the subsonic stagnation flow region, probably causing larger errors than a flow model including recombination.

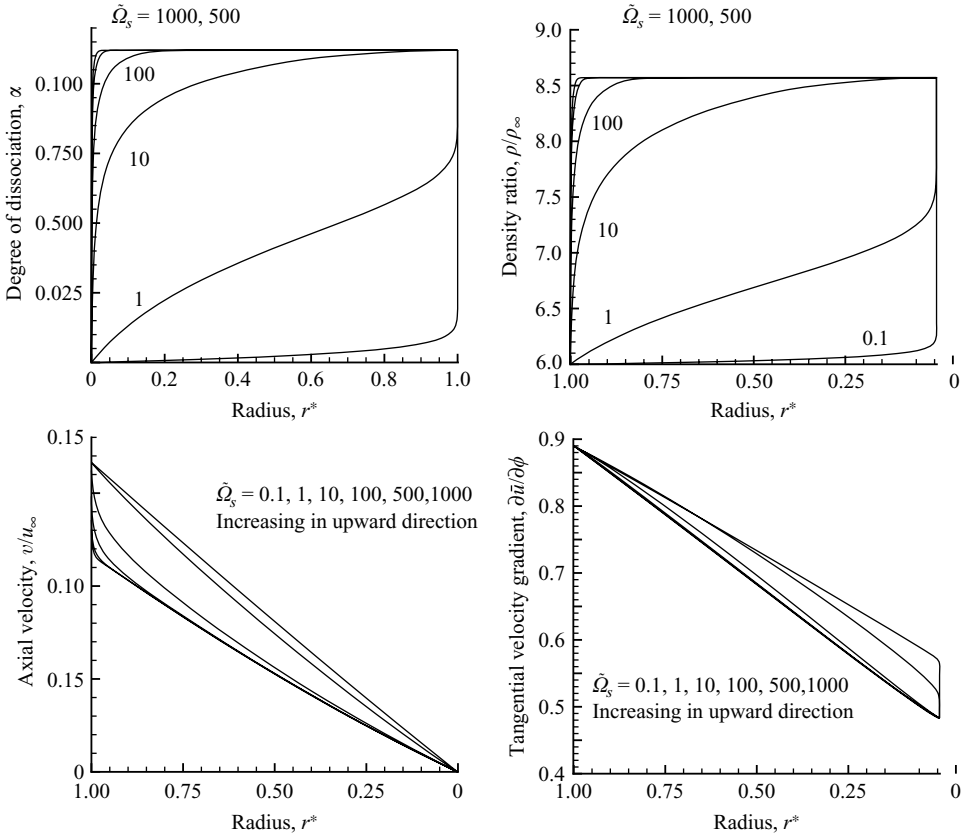

FIGURE 3. Dissociation level, density ratio, axial velocity and tangential velocity gradient along the stagnation line for sphere flow, body $r^* = 0$, shock position $r^* = 1$, $\rho_s/\rho_\infty = 6$, $\rho_s/\rho_b = 0.7$.

3. Results of the theoretical model

For the example of a sphere and for the density ratio $\rho_s/\rho_b = 0.7$ between shock and body, figure 3 shows the profiles of the degree of dissociation, the density, the axial velocity and the tangential velocity gradient. The stagnation point on the body is located at $r^* = 0$ and the shock position is at $r^* = 1$. The reaction rate parameter $\tilde{\Omega}_s$ is defined in (2.3). For the ideal dissociating gas model and for the case of no free-stream dissociation $\alpha_\infty = 0$, this reaction rate parameter can be written as

$$\tilde{\Omega}_s = \left(\frac{\mathrm{d}\rho}{\mathrm{d}t}\right)_s \frac{D}{\rho_s u_\infty} = (2\,\bar{\Theta}_d - 3/2)\Lambda\,\mathrm{e}^{-4\bar{\Theta}_d} \tag{3.1}$$

which, as expected, is directly proportional to Λ, defined in (2.13). It is evident in figure 3 that within a short distance behind the shock the degree of dissociation, the density and the other flow parameters approach their equilibrium value much faster the higher the reaction rate parameter. It is also obvious that independently from the reaction rate parameter at the stagnation point, the flow is locally in equilibrium. This leads for nearly frozen conditions to a very narrow region close to the stagnation point in which the flow comes to equilibrium. The analytical solution for the shock stand-off distance in frozen and equilibrium flow derived by Olivier (2000) assumed

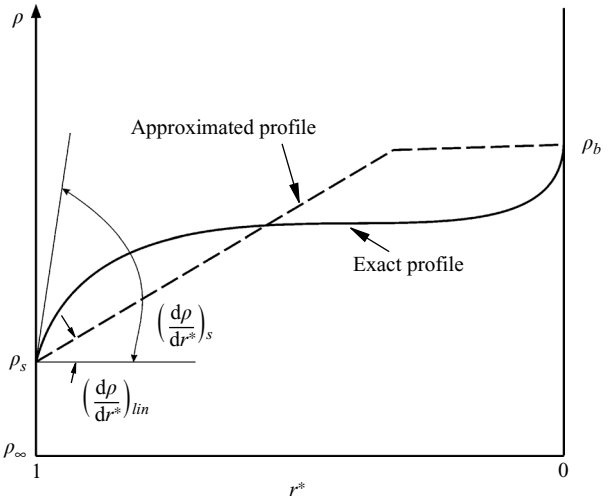

FIGURE 4. Approximation of real density profile by piecewise-linear profile.

a linear behaviour of the tangential velocity gradient between shock and body. In figure 3, it is clear that this assumption approximates the real behaviour quite well.

In order to compare the solution of this method with that given by Wen & Hornung (1995), an equivalent reaction rate parameter has to be determined from a density profile which is based on a piecewise-linear density distribution as in the approach of Wen & Hornung (1995). Choosing the density gradient immediately behind the shock from the real profile for determining the reaction rate as done in (3.1) would result in an overestimation of the reaction rate compared to the model of Wen & Hornung (1995) (see figure 4). Therefore, according to Wen & Hornung (1995) the actual density profile is approximated by piecewise-linear sections. The condition of identical areas below the approximated and the real profile ensures a unique solution. The equivalent reaction rate parameter $\tilde{\Omega}$ then follows from

$$\tilde{\Omega} = \frac{D}{\rho_s u_\infty}\left(\frac{\mathrm{d}\rho}{\mathrm{d}t}\right)_{lin} = 2\left(\frac{\rho_\infty}{\rho_s}\right)^2\left[\frac{\mathrm{d}(\rho/\rho_\infty)}{\mathrm{d}\bar{r}}\right]_{lin}. \tag{3.2}$$

In figure 5 the scaled shock stand-off distance (2.2) is plotted versus the reaction rate and the additional parameter given by the density ratio between shock and body. For the solution of the governing equations given above, the shock curvature parameter $\partial\beta/\partial\phi$ for the stagnation streamline must be known. This value has been determined by adapting the solution for the frozen case to the value given by Lobb (1964), i.e. $\tilde{\Delta} = 0.41$ which for non-reactive hypersonic flow approximates very accurately the numerical solution of Van Dyke (1958), see figure 1. The value of the shock curvature parameter thus determined is to 0.11 and has been kept constant for the whole reactive flow regime. The value 0 would describe a perfect circular shock shape at the stagnation point. In this case, the non-dimensionalized shock stand-off distance is $\tilde{\Delta} = 0.4$. The small deviation between this value and that resulting from Van Dyke's solution ($\tilde{\Delta} = 0.41$) demonstrates the small correction by the shock curvature parameter.

In spite of the quite different models applied, the agreement between the approach of Wen & Hornung (1995) and the present method is very good. Of course, the stretching of the curves shown in figure 5 by the reaction rate parameter $\tilde{\Omega}$ depends on the

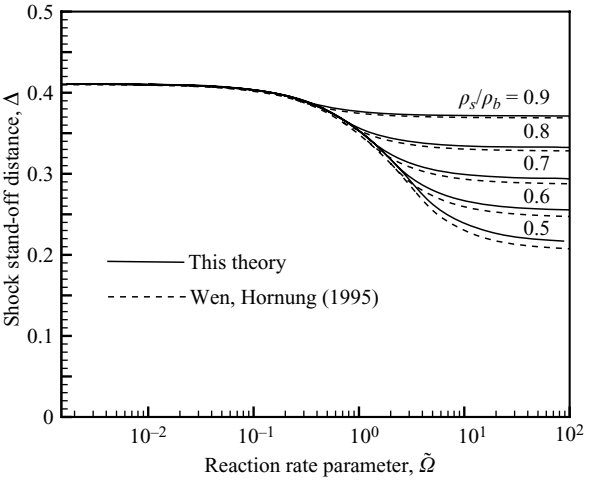

FIGURE 5. Scaled shock stand-off distance as function of reaction rate parameter $\tilde{\Omega}$, $\rho_\infty/\rho_s = 1/6$.

evaluation of an equivalent density gradient approximating the real density profile between shock and body by a piecewise-linear one. For comparing experimental or numerical results with those given by the theory, in principle the reaction rate parameter can be determined for a density gradient at any position between shock and body. The largest relative deviation between the results of the theory presented and Wen & Hornung's theory is 5 % and occurs for the lowest density ratio for equilibrium flow conditions. This quite good agreement achieved between the present method, utilizing the ideal dissociating gas model, and Wen & Hornung's model which does not require the choice of any gas model, indicates that within the given accuracy the details of the gas model considered have little influence on the description of the shock stand-off phenomenon, provided that the most important reactive mechanisms like dissociation, recombination, dependence of reaction rate on local flow properties, etc. are captured. In the following, this is also demonstrated by comparing the numerical solution for air in fully thermal and chemical non-equilibrium and the result of this theory. In this case, the deviation between the theoretical model here presented assuming the ideal dissociating gas model, and the numerical solution for reactive air 7 %. This deviation becomes even smaller if in the numerical solution the physical modelling of the high-temperature phenomena is adapted to the ideal dissociating gas model. In this case, the deviation is only 2 %.

In contrast to the approach of Wen & Hornung (1995) the model presented here does not require a fitting of different solutions depending on the value of the reaction rate parameter. A uniform solution is achieved that is valid for the whole flow regime ranging from frozen up to equilibrium flow. As expected and discussed by Wen & Hornung (1995) for increasing reaction rate parameter, i.e. approaching the equilibrium flow regime, the shock stand-off distance becomes smaller with increasing density at the stagnation point or decreasing density ratio ρ_s/ρ_b. In this case, the average density between shock and body is larger, resulting in a smaller shock stand-off distance. From physical reasoning it is also expected that the strongest dependence of the stand-off distance on the reaction rate parameter occurs for the non-equilibrium regime, i.e. in figure 5 for reaction rate parameters ranging from 0.1

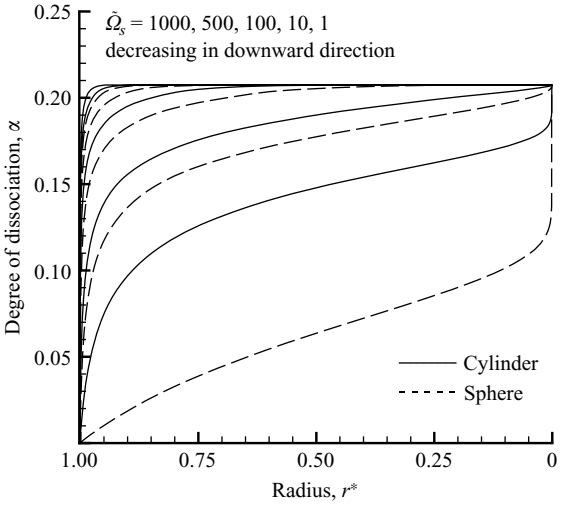

FIGURE 6. Dissociation level along stagnation streamline for cylinder and sphere, $\rho_s/\rho_b = 6$.

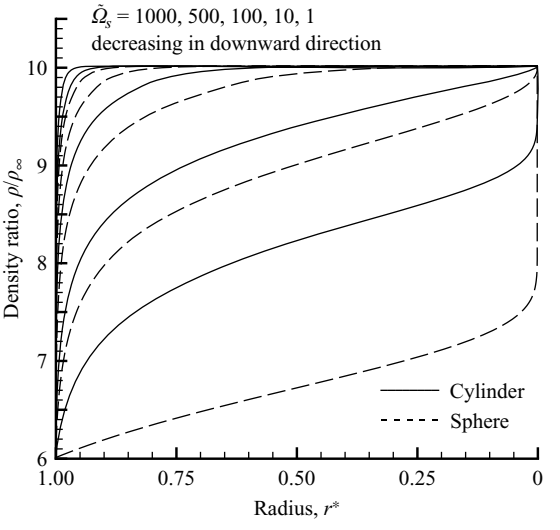

FIGURE 7. Density ratio along stagnation streamline for cylinder and sphere, $\rho_s/\rho_b = 6$.

to 10. In accordance with the features of reactive systems, the dependence on the reaction rate diminishes for frozen and equilibrium conditions.

There are some notable differences between the radial profiles for the flow around a sphere and a cylinder. For the cylinder, especially for low reaction rates, the degree of dissociation and the density are significantly larger than for the sphere (see figures 6 and 7). Not only does the magnitude of these values differ, but also their qualitative behaviour. Whereas for the sphere for low reaction rates behind the shock, the degree of dissociation and the density show a moderate rise, for the cylinder much larger gradients are obvious. With increasing reaction rate, the differences between the radial profiles diminish. Also, the tangential velocity gradient in the case of a cylinder shows a quite different behaviour from that for a sphere (see figure 8). Its absolute magnitude is less, which results in a larger shock stand-off distance. But furthermore, near the

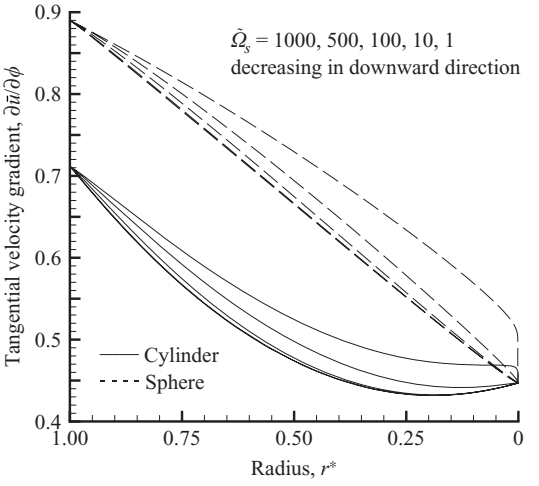

FIGURE 8. Tangential velocity gradient along stagnation streamline for cylinder and sphere, $\rho_s/\rho_b = 6$.

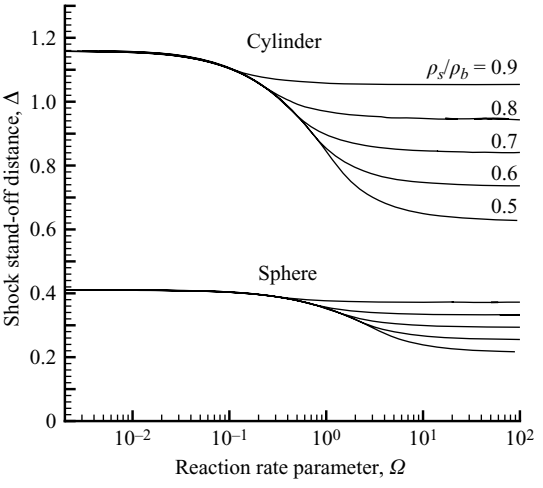

FIGURE 9. Shock stand-off distance for cylinder and sphere, $\rho_s/\rho_b = 6$.

body its shape differs significantly from that for a sphere. For a small reaction rate parameter, a local minimum of the tangential velocity gradient occurs close to the stagnation point. As expected, the scaled shock stand-off distance for a cylinder show qualitatively the same behaviour as for the sphere (see figure 9), but, as is well known, with a more than doubled stand-off distance.

The method described can easily be extended to take into account the influence of a finite free-stream dissociation level. This case is of special interest for evaluating experimental results obtained in high-enthalpy facilities like shock tunnels for which freezing of the nozzle flow is of great concern. Fortunately, to discuss the influence of a finite free-stream dissociation it is sufficient to consider the two limiting cases of frozen and equilibrium flow. These are described with sufficient accuracy by the

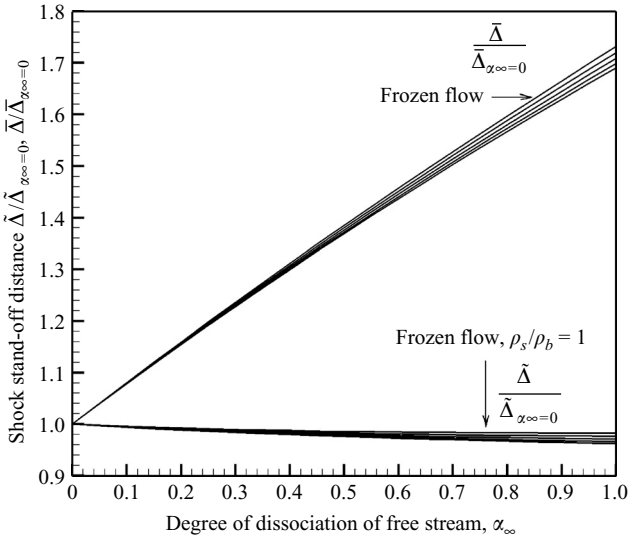

FIGURE 10. Influence of free stream dissociation level on the shock stand-off distance ratio for a sphere. The two sets of curves show the equilibrium flow for $\rho_s/\rho_b = 0.5,\ 0.6,\ 0.7,\ 0.8, 0.9,\ 1.0$ increasing in the upward direction.

analytical solution given by Olivier (2000)

$$\tilde{\Delta} = \left\{ \frac{\rho_s}{\rho_\infty} \sqrt{\frac{1}{4}\left[1 + \left(\frac{\partial \bar{u}}{\partial \phi}\right)_b\right]^2 - \frac{1}{3}\frac{\rho_s}{\rho_b}\frac{\rho_\infty}{\rho_s}\left[1 + 2\left(\frac{\partial \bar{u}}{\partial \phi}\right)_b\right]} - \frac{1}{2}\left[1 + \left(\frac{\partial \bar{u}}{\partial \phi}\right)_b\right]\frac{\rho_s}{\rho_\infty} + \frac{\rho_s}{\rho_b} \right\} \cdot \left(\frac{4}{3} + \frac{2}{3}\left(\frac{\partial \bar{u}}{\partial \phi}\right)_b - 2\frac{\rho_s}{\rho_b}\frac{\rho_\infty}{\rho_s}\right)^{-1}. \tag{3.3}$$

In this relation the free-stream dissociation influences the density jump across the shock which is given for an ideal dissociating gas for the hypersonic limit by

$$\frac{\rho_s}{\rho_\infty} = \frac{7 + \alpha_\infty}{1 + \alpha_\infty}. \tag{3.4}$$

The free-stream dissociation causes a reduced density jump across the shock resulting in a bigger stand-off distance. Relations (3.3) and (3.4) allow evalution of the influence of the free-stream dissociation on the stand-off distance for frozen flow, $\rho_s = \rho_b$, and for equilibrium. In the latter case, the value of the density ratio ρ_s/ρ_b is prescribed as a parameter. Figure 10 shows the stand-off distance in the case of free-stream dissociation scaled with the stand-off distance for no free-stream dissociation. For this ratio of stand-off distances the difference between frozen and equilibrium flow is in general not very large but grows with increasing dissociation level. It is interesting to note that for the stand-off ratio

$$\frac{\tilde{\Delta}}{\tilde{\Delta}_{\alpha_\infty=0}} = \frac{\bar{\Delta}}{\bar{\Delta}_{\alpha_\infty=0}} \frac{\rho_s/\rho_\infty}{(\rho_s/\rho_\infty)_{\alpha_\infty=0}} \tag{3.5}$$

the influence of the free-stream dissociation is very weak. But for the geometrical stand-off distance ratio $\bar{\Delta}/\bar{\Delta}_{\alpha_\infty=0}$ there is a nearly linear dependence on the free-stream dissociation level. For a free-stream dissociation of e.g. 20 % the stand-off

distance is about 16 % larger than for the case without pre-dissociation, because according to (3.4) the free-stream dissociation leads to a smaller density jump across the shock. This shows clearly that the influence of a possible free-stream dissociation in high-enthalpy wind tunnels must be considered, especially comparing experimental and numerical results or data obtained in different wind tunnels.

4. Physical and numerical model for detailed flow field study

It is generally assumed that the shock detachment distance only weakly depends on the physical model used to describe real gas effects, in particular vibrational and chemical non-equilibrium. Thus, a model of the Lighthill type (Freeman 1958) described above may be sufficient if a precision of about 10 % is sufficient. In the same way, the well-known model of Park (1989*a*, *b*), also simple to implement, can be sufficient to yield the same magnitude of accuracy. This was supported by relatively old measurements (Lobb 1964) which partially suffered from experimental shortcomings. However, recent measurements carried out with sophisticated techniques of diagnostics allowed results of higher precision of about 5 % (Furudate, Nonaka & Sawada to be obtained 1999; Hashimoto 2003). These experimental results lead to the conclusion that the values of the shock detachment distances measured on hemispherical models are larger than those deduced from Park's model and thus closer to the frozen case. These measurements also show that the older values previously mentioned are smaller and that the difference can be ascribed to an insufficient purity of the test gas used in these early experiments. These considerations lead to the conclusion that to achieve a high accuracy a more realistic physical model must be used for a complete calculation of the hypersonic flow around axisymmetrical bodies and, in particular, of the shock detachment distance in front of these bodies. This model must also take into account the simultaneous influence of the vibrational excitation and the chemical reactions as well as their interaction. These phenomena are largely present under the experimental conditions referred to above, i.e. for enthalpies ranging between 5 and 15 MJ kg^{-1}. For simplicity and clarity, first the case of dissociation of pure diatomic gases is considered and thereafter the case of complex gases and gas mixtures.

4.1. *Physical model of non-equilibrium flow*

4.1.1. *Pure diatomic gases*

For a pure diatomic gas of species A which is partially dissociated, the reactions considered are the following:

$$A_2 + A_2 \rightleftharpoons A_2 + A + A, \tag{4.1}$$

$$A_2 + A \rightleftharpoons A + A + A. \tag{4.2}$$

Constants K_{D1} and K_{D2}, respectively, are the rate constants of the dissociation reactions (4.1) and (4.2), K_{R1} and K_{R2} the rate constants of the corresponding recombination reactions. To this set of reactions, one must add the 'reactions' of vibrational excitation and de-excitation of molecules A_2 for which one single relaxation time τ_v will be considered.

Thus, considering atoms A and vibrationally excited molecules A_2 in non-equilibrium situations, the Boltzmann equation for the distribution function of the molecules f_i may be written by splitting the collisional term J into three parts: J_{tr} that includes the translation–translation exchanges (elastic terms) and translation–rotation exchanges, J_v that includes all vibrational exchanges and J_c that includes the chemical exchanges with dissociation and recombination terms J_D and J_R,

respectively: $J_c = J_D - J_R$. It is assumed that $\tau_{tr} \ll \tau_v$ and τ_c, where hese symbols represent the characteristic relaxation times of the corresponding collisional terms. This is valid for most high-temperature flows in which τ_v generally remains smaller than τ_c, such as for nitrogen, or comparable, such as for high-temperature oxygen. Thus, for molecules at level i, including a rotational level i_r and a vibrational level i_v,

$$\frac{\mathrm{d}f_{ip}}{\mathrm{d}t} = J_{trp} + J_{vp} + J_{cp}. \tag{4.3}$$

For atoms, (4.3) simplifies to

$$\frac{\mathrm{d}f_q}{\mathrm{d}t} = J_{tq} + J_{cq}, \tag{4.4}$$

where the indices p and q, respectively, denote molecules and atoms. If (4.3) and (4.4) are multiplied by their general collisional invariants, then integrated on the velocity space, summed over the rotational and vibrational levels and finally added, one obtains the three usual global conservation equations for mass, momentum and energy governing the mixture consisting of A and A_2:

$$\frac{\partial \rho}{\partial t} + \frac{\partial \rho \boldsymbol{V}}{\partial \boldsymbol{r}} = 0, \tag{4.5}$$

$$\rho \frac{\mathrm{d}\boldsymbol{V}}{\mathrm{dt}} = -\frac{\partial p}{\partial \boldsymbol{r}} - \frac{\partial \boldsymbol{\tau}}{\partial \boldsymbol{r}}, \tag{4.6}$$

$$\rho \frac{\mathrm{dh}}{\mathrm{dt}} = \frac{\mathrm{dp}}{\mathrm{dt}} - \frac{\partial \boldsymbol{q}}{\partial \boldsymbol{r}} - \boldsymbol{\tau} : \frac{\partial \boldsymbol{V}}{\partial \boldsymbol{r}}, \tag{4.7}$$

where p, ρ, $\boldsymbol{V}$, h, $\boldsymbol{\tau}$, $\boldsymbol{q}$, respectively, represent the pressure, density, velocity, enthalpy, stress tensor and heat flux of the mixture.

In order to complete these equations, the vibrational energy conservation equation and species conservation equations for the molecules and atoms are obtained by multiplying (4.3) and (4.4), respectively, by ε_{iv}, the vibrational energy of level i_v, and the molecular mass m_p. As before, these equations are integrated and summed over the internal levels. For a more detailed analysis, one can consider the balance of molecules at each vibrational level, but this is not necessary for a global view. In the same way, the assumption of the harmonic oscillator model may be retained. These equations are as follows:

$$\frac{\partial \rho_p}{\partial t} + \frac{\partial \rho_p \boldsymbol{V}_p}{\partial \boldsymbol{r}} = \dot{w}_p, \tag{4.8}$$

$$\rho_p \frac{\mathrm{de_{vp}}}{\mathrm{dt}} + \frac{\partial \boldsymbol{q}_{vp}}{\partial \boldsymbol{r}} = \dot{e}_{vp} + \dot{w}_{vp}, \tag{4.9}$$

with

$$\dot{e}_v = \frac{e_v - \bar{e}_v}{\tau_v} \quad \text{and} \quad \tau_v^{-1} = \sum_{m=p,q} \xi_m \tau_{pm}^{-1},$$

where $\dot{w}_p$ and $\dot{w}_{vp}$ are source terms for the mass and the vibrational energy of species $p(A_2)$ due to reactive collisions; e_v and q_v describe the vibrational energy and the corresponding heat flux, $\bar{e}_v$ the equilibrium vibrational energy and $\dot{e}_v$ the vibrational energy production due to non-reactive collisions. Furthermore, the mass production term is given by

$$\frac{\dot{w}_p}{M_p} = \frac{\dot{w}_{Rp} - \dot{w}_{Dp}}{M_p} = \left(K_{R1} X_p X_q^2 + K_{R2} X_q^3\right) - \left(K_{D1} X_p^2 + K_{D2} X_p X_q\right) \tag{4.10}$$

and the production term for the vibrational energy by

$$\dot{w}_v = (e_v - e_{vR})\dot{w}_R - (e_v - e_{vD})\dot{w}_D\,, \tag{4.11}$$

where e_{vR} and e_{vD} are the vibrational energies gained or lost per recombination and dissociation reaction, respectively. X is the molar concentration. The rate constants are determined by

$$K_D = \sum_{ip} k_{Di_p}\xi_{i_p} \tag{4.12}$$

with $\xi_{i_p} = n_{i_p}/n_p = X_{i_p}/X_p$.

The expressions for K_R, K_D, e_{vR} and e_{vD} have to be determined to close the complete set of equations, and it is the same for all transport terms ($\boldsymbol{V_p}, \boldsymbol{\tau}, \boldsymbol{q}$) appearing in the conservation equations (4.5), (4.6) and (4.7). These may be obtained from a generalized Chapman–Enskog (GCE) procedure summarized below (Kogan, Galkin & Makashev 1979; Brun, Villa & Meolans 1984).

Thus, assuming as usual that τ_v remains smaller than τ_c and much smaller than the reference flow time δ, f_{ip} is expanded in a series of the 'small' parameter $\varepsilon = \tau_v/\delta$. Excluding the regions where steep gradients prevail, the method applies to vibrational and chemical non-equilibrium zones up to complete equilibrium. Truncating the expansion to the first order, the Boltzmann equation (4.3) is replaced by the following system giving successively the zeroth- and first-order expressions for f_{ip}:

$$J^0_{trvp} = 0, \tag{4.13}$$

$$\frac{\mathrm{d}f^0_{ip}}{\mathrm{d}t} = J^1_{trvp} + J^0_{cp} + J^1_{cp}. \tag{4.14}$$

A similar but simpler system is obtained for f_{iq}.

Equation (4.13) gives a zeroth-order solution for f^0_{ip} in translational–rotational–vibrational equilibrium and in chemical non-equilibrium. Then, the first-order solution deduced from (4.14) may be written $f^1_{ip} = f^0_{ip}(1+\varphi_{ip})$, where the perturbation φ_{ip} takes into account translational–rotational non-equilibrium which is the origin of most transport terms, vibrational non-equilibrium and interactions between vibrational and chemical non-equilibrium. Thus, φ_{ip} may be written in the following general form:

$$\varphi_{ip} = A\boldsymbol{c}\frac{\partial T}{\partial \boldsymbol{r}} + B\boldsymbol{cc}\frac{\partial \boldsymbol{V}}{\partial \boldsymbol{r}} + D\frac{\partial \boldsymbol{V}}{\partial \boldsymbol{r}} + G + H\boldsymbol{c}\frac{\partial \xi}{\partial \boldsymbol{r}}\,, \tag{4.15}$$

where $Y = A, B, D, G, H$ are scalar functions related to conductivity, shear and bulk viscosities, relaxation pressure and diffusion, respectively. Each Y term is expanded in Sonine–Wang Chang–Uhlenbeck polynomials

$$Y = \sum_{m,n,p} y_{mnp} S_t^m P_r^n P_v^p \tag{4.16}$$

with $Y = A, B, D, G, H$. Only zeroth- and first-order terms are retained in the expansion (4.16), i.e. y_{000}, y_{100}, y_{010}, y_{001}, where each subscript corresponds to the order of expansion for translation, rotation and vibration, respectively. These terms depend on collisional integrals, generally well-known with various degrees of approximation. In this way, the transport coefficients are deduced from the corresponding expressions.

On the other hand, it is easily verified that the non-equilibrium rate constants K_D and K_R defined by (4.12) are linear functions of D and G terms, and this is the same for the non-equilibrium vibrational energy e_v. Eliminating these terms from the

functions, explicit relations between the rate constants and the vibrational energy are obtained. Thus, we find for K_D (Belouaggadia & Brun 1998)

$$\frac{K_D - \bar{K}_D}{\bar{K}_D} = \left(\frac{e_v - \bar{e}_v}{\bar{e}_v}\right)\left(\frac{e_{vD} - \bar{e}_v}{\bar{e}_v}\right), \tag{4.17}$$

where e_{vD} represents the vibrational energy lost per dissociation of each molecule and $\bar{K}_D$ is the Arrhenius rate constant of the reaction considered with $\bar{K}_D = \bar{K}_D(T)$. More details may be found in Belouaggadia & Brun (1998). The loss of vibrational energy per dissociation of each molecule may be computed from its definition, i.e.

$$e_{vD} = \frac{\sum_{i_v} \int J_D(\varepsilon_{i_v}/m)\,\mathrm{d}c}{\sum_{i_v} \int J_D\,\mathrm{d}c}. \tag{4.18}$$

An oscillator model including dissociation is needed for computing e_{vD}. Thus, if the equiprobable, i.e. non-preferential, model is used to determine the specific dissociation rate constants K_{Di_p}, at the zeroth order of the distribution function ($e_{vD} = \bar{e}_{vD}$) we find a value for e_{vD} close to $0.5e_D$ for the harmonic oscillator model and close to $0.4e_D$ for the anharmonic one. For example, e_{vD} for N_2 is $0.44e_D$ and for O_2 is $0.42e_D$. At the first order of the distribution function, a more complex expression is obtained, but an approximate value of $0.3e_D$ can be used instead of that complete expression. This value is close to that generally recommended (Park 1990).

For the recombination parameter e_{vR}, it is assumed that $e_{vR} = \bar{e}_{vD}$ for the backward reaction (4.1) and $K_R = \bar{K}_R$ for the reaction (4.2), which means that the recombination involving only atomic species is not influenced by the vibrational state of the recombined molecules. This is a commonly used assumption (Treanor & Marrone 1962). Finally, the Navier–Stokes equations completed by (4.8) and (4.9) have to be solved. In these equations, Arrhenius rate constants are taken from Park (1985) and vibrational relaxation times from Millikan & White (1969). The transport terms, rather than being directly calculated are written as functions of the viscosity and of the non-dimensional numbers, namely the frozen Prandtl, the Lewis and vibrational numbers. These quantities are weakly sensitive to non-equilibrium conditions (Brun 1988).

4.1.2. *Extension to gas mixtures*

In the case of complex gases or gas mixtures, many reactions may take place. The general equations (4.7) to (4.9) remain valid of course, but the source terms are to be deduced from the set of s chemical reactions of the following type:

$$\sum_p \nu'_{ps} A_p \rightleftharpoons \sum_p \nu''_{ps} A_p. \tag{4.19}$$

The chemical and vibrational energy source terms are given by

$$\dot{w}_p = \sum_s (\dot{w}_{pfs} - \dot{w}_{pbs}) = \sum_s M_p\left(\nu^*_{ps} - \nu'_{ps}\right)\left(K_{fs}\prod N_p^{\nu'_{ps}} - K_{bs}\prod N_p^{\nu''_{ps}}\right) \tag{4.20}$$

and

$$\dot{w}_{Vp} = \sum_s \left[\left(e_{Vp} - e_{Vpfs}\right)\dot{w}_{pfs} - \left(e_{Vp} - e_{Vpbs}\right)\dot{w}_{pbs}\right]. \tag{4.21}$$

As in the case of dissociating pure gases, the expressions for K_{fs}, K_{bs}, e_{Vpfs} and e_{Vpbs} have to be determined in order to close the complete set of equations (4.7) to (4.9). In particular, the rate constants K_s may be written in the form

$$K_s = Z_s \bar{K}_s, \tag{4.22}$$

where $\bar{K}_s$ represents the Arrhenius rate constant of the reaction s, and

$$Z_s = \left(\frac{e_{vp} - \bar{e}_{vp}}{\bar{e}_{vp}}\right)\left(\frac{e_{vps} - \bar{e}_{vp}}{\bar{e}_{vp}}\right). \tag{4.23}$$

Among the reactions described by (4.19), are dissociation and recombination as in the case of pure gases, but also various exchange reactions for which terms like e_{vps}, the vibrational energy of the species p lost per forward or backward reaction, must be evaluated. They generally represent a fraction of the activation energy, also depending on the oscillator model (Belouaggadia & Brun 2006).

In the case of complex mixtures, it is necessary to take into account the VV-transitions between different molecular components (Stupochenko *et al* 1967), even if the harmonic oscillator model is retained for the TV-transitions (Millikan & White 1969). Taking this into account, the Navier–Stokes equations are written in a way similar to the case of pure gases (Brun 1991; Pascal & Brun 1993). They are completed by species conservation equations and vibrational relaxation equations modified as specified above. This complete set of equations is solved for the geometry and flow conditions considered.

5. Numerical simulation

In a cylindrical coordinate system (x, y) the governing equations describing the unsteady viscous flow of the non-equilibrium mixture (A, A_2) as defined above, may be expressed in the following vectorial form:

$$\frac{\partial \boldsymbol{U}}{\partial t} + \frac{\partial \boldsymbol{F}}{\partial x} + \frac{\partial \boldsymbol{G}}{\partial y} + \boldsymbol{H} = \boldsymbol{\Omega}, \tag{5.1}$$

where the conservative vector $\boldsymbol{U}$ includes the unknown quantities

$$\boldsymbol{U} = (\rho_p, \rho_q, \rho u, \rho v, \rho e, \rho_p e_{vp}).$$

$\boldsymbol{F}$ and $\boldsymbol{G}$ are the vectors that include the convective and diffusive fluxes in each direction x and y. The vector $\boldsymbol{H}$ includes the axisymmetrical terms of the equations, and $\boldsymbol{\Omega}$ contains the chemical and vibrational energy source terms.

The unsteady equations (5.1) have to be integrated for the flow field considered, starting from initial conditions and taking into account the usual boundary conditions. In this way, a time-eveloping solution is obtained until the required steady state is achieved. The numerical method is carried out on a rectangular plane ξ, η, derived from the physical plane x, y by a suitable transformation. The system of equations (5.1) is solved by an implicit finite difference scheme. For each node (i, j) at the time step $(n+1)\Delta t$, the system may be written in the following form:

$$\frac{\boldsymbol{U}^{(n+1)} - \boldsymbol{U}^{(n)}}{\Delta t} + \frac{\mathrm{D}}{\Delta \xi}(\boldsymbol{F}_e + \boldsymbol{F}_d)^{(n+1)} + \frac{\mathrm{D}}{\Delta \eta}(\boldsymbol{G}_e + \boldsymbol{G}_d)^{(n+1)} + \boldsymbol{H}^{(n+1)} = \boldsymbol{\Omega}^{(n+1)}, \tag{5.2}$$

where $\boldsymbol{F}_e$ and $\boldsymbol{G}_e$ represent the Eulerian convective fluxes, $\boldsymbol{F}_d$ and $\boldsymbol{G}_d$ include transport terms and D/Δ are finite difference operators. Each vector Φ of (5.2) is linearized in

the form

$$\Phi^{(n+1)} = \Phi^{(n)} + \left(\frac{\partial \Phi}{\partial U}\right)^{n} \left(U^{(n+1)} - U^{n}\right), \tag{5.3}$$

where $\partial\Phi/\partial U$ is the Jacobian matrix. Then, having split F_e and G_e into a positive and a negative part, the system (5.2) is written in the form

$$\left[I + \Delta t \left(\frac{\mathrm{D}_+ A_-}{\Delta\xi} + \frac{\mathrm{D}_- A_+}{\Delta\xi} + \frac{\mathrm{D}^2 S_\mathrm{d}}{\Delta\xi^2} + \frac{\mathrm{D}_+ B_-}{\Delta\eta} + \frac{\mathrm{D}_- B_+}{\Delta\eta} + \frac{\mathrm{D}^2 R_\mathrm{d}}{\Delta\eta^2} + K + L\right)\right] \times \left(U^{(n+1)} - U^{n}\right) = \Delta U^{(n)}, \tag{5.4}$$

where

$$\Delta U^{(n)} = -\Delta t \left(\frac{\mathrm{D} F^{(\mathrm{n})}}{\Delta\xi} + \frac{\mathrm{D} G^{(\mathrm{n})}}{\Delta\eta} + H^{(n)} - \Omega^{(n)}\right). \tag{5.5}$$

The symbols D, D_+, and D_- denote central, forward and backward difference operators, respectively. A_-, A_+, S_d, B_-, B_+, R_d, K and L are the Jacobian matrices, respectively, of F_e^-, F_e^+, F_d, G_e^-, G_e^+, G_d, H and Ω. After discretization, the system may be written as a linear system with a pentadiagonal matrix. At each time step, a predictor–corrector scheme is used and the system is solved by a Gauss–Seidel line relaxation method (MacCormack & Candler 1989) with alternating sweeps in backward and forward in direction ξ.

A few thousand grid points with varying grid spacing are generally required for various meshes (typically 60×80 grid points), with $\Delta x_{min} \approx 10^{-5}$ m and $\Delta y_{min} \approx 10^{-8}$ m. The time step is calculated from a stability criterion based on the CFL criterion (MacCormack & Baldwin 1975) where the implicit method allows the use of CFL numbers ranging from 1 to 60. Close to the symmetry axis, the mesh size is progressively decreased in order to determine the shock position with high accuracy. Moreover, the 'numerical thickness' of the shock is estimated by using the Prandtl definition, i.e.

$$\delta_{Pr} = (\rho_b - \rho_a) \Big/ \left(\frac{\mathrm{d}\rho}{\mathrm{dx}}\right)_{max} \quad \text{or} \quad \delta_{Pr} = (T_b - T_a) \Big/ \left(\frac{\mathrm{dT}}{\mathrm{dx}}\right)_{max}. \tag{5.6}$$

This thickness may be considered as the maximum error of the shock position, assumed to be located at the position of maximum slope of the density $\rho(x)$ or temperature $T(x)$ distribution along the axis of symmetry. The error in the shock position estimated in this way amounts to less than 5 %.

During the first phase of the simulation the solution shows an unsteady behaviour (see figure 11). But after a few hundred time steps the solution becomes stationary and the value for the shock stand-off distance can be determined.

The grid dependence has been studied for three meshes with 50×50, 60×60 and 80×80 grid points. For the coarse mesh the stand-off distance normalized with the sphere radius is 0.131 and for the last two meshes is 0.1309. Therefore, for the problem considered meshes with 60×60 grid points or even more can be regarded as yielding a mesh-independent solution.

6. Results and comments

Any new modelling of physical phenomena must be compared to other existing models and validated with reliable data. Thus, computations of the whole flow field around hemispherical bodies using the model presented here have been performed,

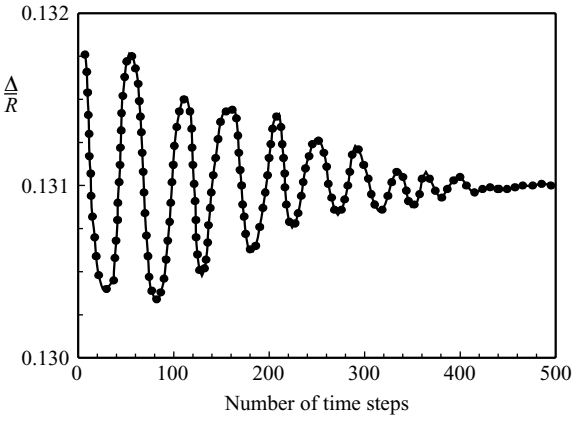

FIGURE 11. Evolution of the shock stand-off distance as function of the number of time steps, $\rho_s/\rho_b = 0.7$, frozen flow

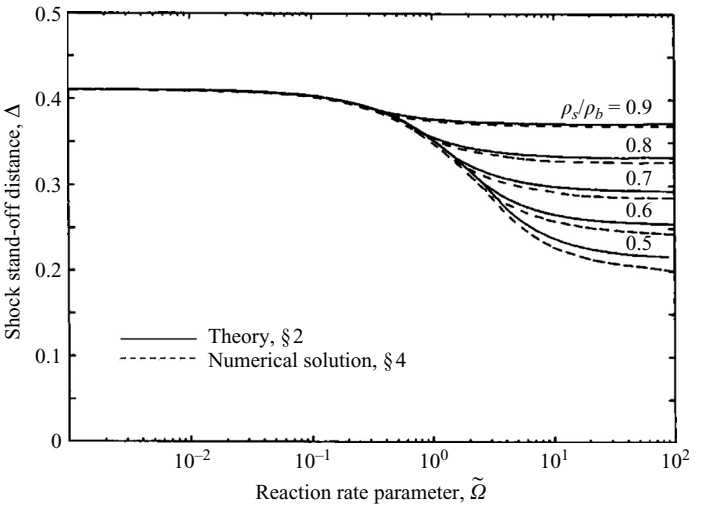

FIGURE 12. Comparison of shock stand-off distances for a sphere.

and the resulting values for the shock stand-off distances are compared to the results of the theoretical model described in § 2 and to recent experimental measurements.

These experimental results have been obtained in shock tunnels and gun tunnels working in non-equilibrium conditions and with high stagnation enthalpies. Excluding the oldest experiments for the reasons previously described, the most significant experiments have been conducted by Wen & Hornung (1995), Nonaka (2000) and Hashimoto (2003).

6.1. *Comparison with the theoretical model*

The most important result of the theoretical model described in § 2 is the universal representation of the non-dimensional shock stand-off distance as a function of a rate parameter and of the density ratio ρ_s/ρ_b. This behaviour is also found in the numerical simulation. Figures 12 and 13 show a comparison of the shock stand-off distance $\tilde{\Delta}$ between the numerical results obtained with the present model and

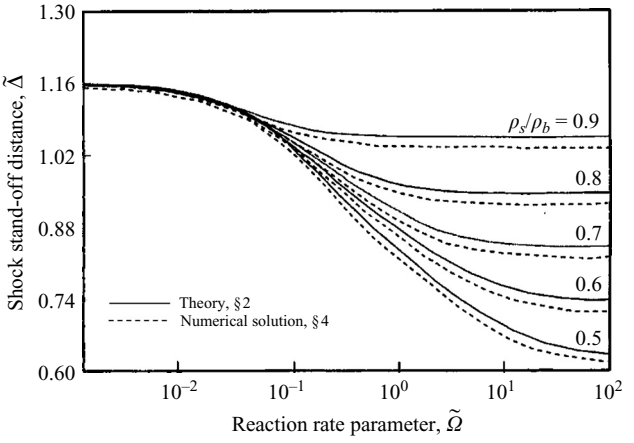

FIGURE 13. Comparison of shock stand-off distances for a cylinder.

the theoretical results of §2 for spherical and cylindrical bodies, respectively. Pure nitrogen has been used as gas for the numerical simulation.

For the hemispherical case (figure 12), the discrepancies between the two models, though not important, increase with the decrease of the density ratio, i.e. with increasing dissociation, and the maximum deviation is close to 7 %. The difference is reduced to less than 2 % if, in the present computation, the Arrhenius values for the rate constants are used, the relaxation equation is suppressed, and the vibrational energy is taken as half of the local equilibrium value. In this way the current model is as far as possible adapted to Lighthill's model (Freeman 1958). This result, therefore, shows that the main source of disagreement comes from the use of the ideal dissociating gas assumption in the theoretical model. Furthermore, it is important to note that the approximate theory of Wen & Hornung gives values close to those given by the present model with a deviation of about 3 %.

For the cylindrical case (figure 13), the difference between the models is generally similar to the spherical case, but the discrepancies do not increase with decreasing density ratio ρ_s/ρ_b. The difference between the two models, however, as previously, would become negligible if a more realistic physical model were included in the theoretical model. However, introducing more realistic and therefore more complex models into the theoretical approach would significantly reduce the possibility of describing the most important physical phenomena by analytical expressions extracted from the set of governing equations. From another point of view, for the cylindrical case, the much larger shock stand-off distance makes it regrettable that, to our knowledge, so few experimental results are available. The larger shock stand-off distance at the cylinder reduces the relative error in the measurements.

6.2. *Comparison with Wen & Hornung's experiments*

In these experiments, the shock stand-off distance is measured by a conventional interferometric method in front of spheres of 1 to 6 in. in diameter which are placed at the exit of a contoured nozzle with 300 mm exit diameter. The experiments have been performed in a free piston shock tunnel capable of producing flows of nitrogen, air and carbon dioxide up to stagnation enthalpies of 25 $\mathrm{MJ\,kg^{-1}}$. The measured values of the non-dimensional shock stand-off distance are given as a function of the

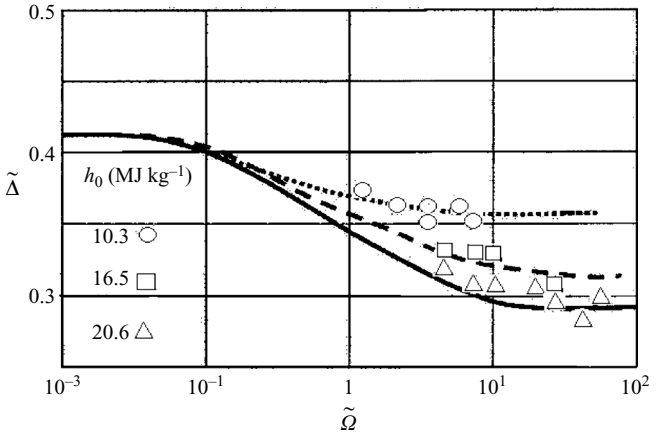

FIGURE 14. Comparison of measured stand-off distances, symbols (Wen & Hornung 1995), with the present model (air), solid and broken lines.

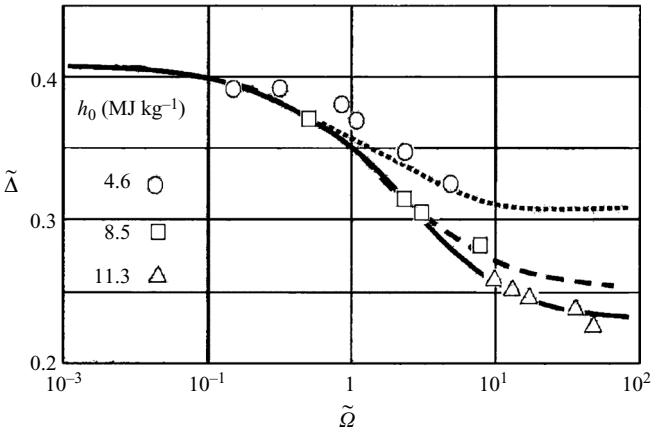

FIGURE 15. As figure 14 but for carbon dioxide.

general reaction rate parameter

$$\tilde{\Omega} = \left(\frac{\mathrm{d}\rho}{\mathrm{dt}}\right)_s \frac{D}{\rho_s u_\infty}$$

which is defined as part of an approximate theory (Wen & Hornung 1995). The values of the shock stand-off distance found for various total enthalpies are represented in figures 14 and 15, respectively, for air and carbon dioxide flows and compared with values given by the present model.

For the computation of the air flow, as usual a mixture of five species is considered (N_2, O_2, NO, N, O). In the same way, 15 dissociation and recombination reactions of the molecular species and two exchange reactions involving NO are considered, so that 34 reactions are taken into account with rate constants given by (4.23). However, six recombination reactions involving atoms only cannot be described by the present model. This is consistent with the hypothesis, usually assumed, of the independence of these reactions from the vibrational distribution of the recombined molecules (Park 1990). Arrhenius rate constants are taken from Park (1989*a*), and

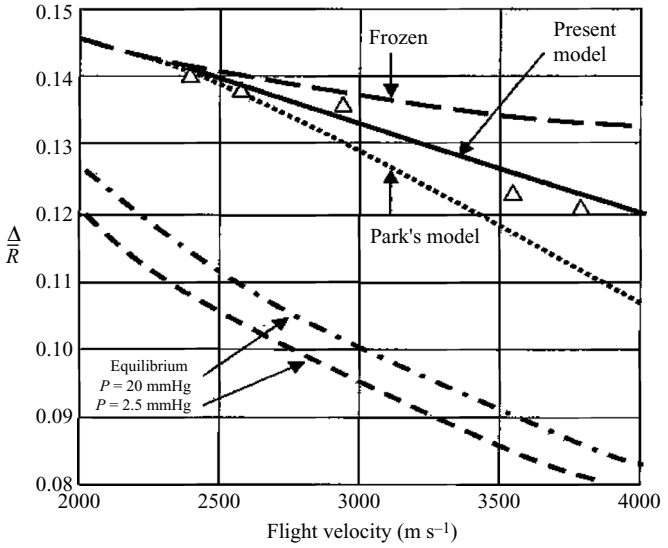

FIGURE 16. Comparison between measured and computed shock stand-off distance, $\rho_\infty R = 1 \times 10^{-4}$ kg m^{-2}, △: experimental values.

TV and VV relaxation times, respectively, from Millikan & White (1969) and from Stupochenko *et al* (1967). For the computation of the carbon dioxide flow, five species are considered (CO_2, O_2, CO, C, O) and 12 reactions are taken into account. Arrhenius rate constants and TV relaxation rates are taken from Mazoue, Chikhaoui & Brun (1994). As expected, the non-equilibrium effects are more important for carbon dioxide, because of its low dissociation energy.

Looking at the results given by these experiments and the present model in figures 14 and 15, the agreement seems to be excellent within 5 %, especially when considering the uncertainties of 4 % to 9 % given by the authors for the nominal total enthalpies h_0, which is indirectly determined from measurements of the shock velocity or the stagnation heat flux.

6.3. *Comparison with Nonaka's experiments*

These experiments have been performed in a ballistic range with hemispherical models fired into air as test gas at flight velocities from 5000 to 20 000 m s^{-1}. The nose radii of the models varied from 1 to 15 mm. The shock stand-off distance was measured by shadow and schlieren techniques with an accuracy claimed by the authors of better than 5 %. The experimental shock stand-off distance values, normalized by the nose radius, are given for different values of the scaling parameter $\rho_\infty R$ equal to 1×10^{-4}, 2×10^{-4} and 4×10^{-4} kg m^2, respectively, in figures 16, 17 and 18.

The upper curves represent the well-known solutions previously obtained for frozen flow, $\rho_\infty R = 0$, and the solution for non-equilibrium flow. The lower two curves correspond to the equilibrium solution, $\rho_\infty R = \infty$, obtained for two different ambient pressures. The domain between these two sets of curves represents the non-equilibrium region for finite values of the parameter $\rho_\infty R$.

It is clear that the present experimental data exhibit non-equilibrium effects which become significant with increasing flight velocity while keeping $\rho_\infty R$ constant. In the same way as $\rho_\infty R$ increases, the shock stand-off distance approaches its equilibrium

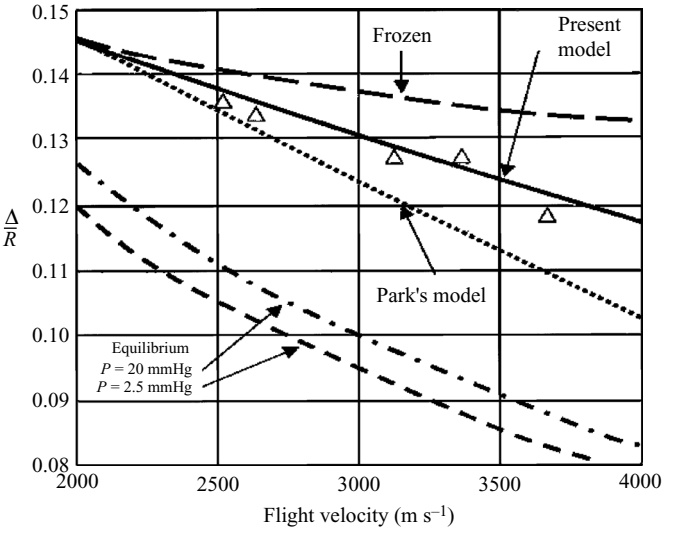

FIGURE 17. Comparison between measured and computed shock stand-off distance, as figure 16 but for $\rho_\infty R = 2 \times 10^{-4}\,\mathrm{kg\,m^{-2}}$.

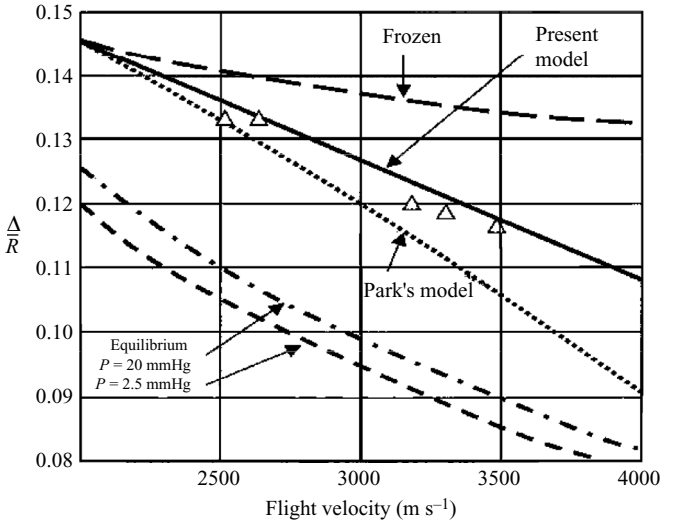

FIGURE 18. Comparison between measured and computed shock stand-off distance, as figure 16 but for $\rho_\infty R = 4 \times 10^{-4}\,\mathrm{kg\,m^{-2}}$.

value. As previously reported and discussed, these results are closer to the frozen case than older data apparently obtained in a contaminated test gas.

A comparison with calculations using the two-temperature model derived by Park (1989*a*, *b*) is also presented in the same figures. As clearly seen, a fair agreement is obtained for nearly frozen flow, i.e. low $\rho_\infty R$ values, and for low velocities. As expected, the agreement is better for nearly equilibrium conditions. However, the computed values gradually depart from the experimental ones as the flight velocity increases and therefore excitation of non-equilibrium effects takes place. For these flow conditions Park's model underestimates the shock stand-off distance. This may be attributed to a relatively slow chemistry associated with an important vibrational

Flow quantities	Condition 1	Condition 2
Nozzle exit conditions:		
Mach number	7.25	6.89
Velocity [m s^{-1}]	4120	2780
Temperature [K]	420	310
T_v (N_2)	2120	1900
T_v (O_2)	900	800
Molar concentrations:		
N_2	0.73	0.70
O_2	0.18	0.13
NO	0.08	0.13
O	0.01	0.04
N	0.00	0.00

TABLE 1. Computed flow conditions at the nozzle exit of Hashimoto's experiments.

relaxation, resulting from the moderate stagnation enthalpies of these experiments which are lower than those of Wen & Hornung's experiments.

The model presented in this paper, which takes this coupling into account, gives values for the shock stand-off distance in good agreement with the experimental data in the whole non-equilibrium regime for the three values of $\rho_\infty R$ considered. The discrepancies between the experimental and numerical results remain less than 4 %.

6.4. *Comparison with Hashimoto's experiments*

The experiments have been performed with hemispherical bodies with radii varying from 12.5 to 5 mm placed at the exit of a conical nozzle with 130 mm exit diameter of a free piston shock tunnel allowing total enthalpies up to 15 M J kg^{-1}. Measurements of the shock stand-off distance have been made by holographic interferometry for two flow conditions 1 and 2 listed in table 1 close to 10 and 5 M J kg^{-1}, respectively.

For comparison with the experimental results, first it was necessary to compute the nozzle flow employing the present model, before computing the flow around the hemisperical bodies. The corresponding flow quantities at the nozzle exit are listed in table 1. As expected, for the nozzle flow a freezing of the mass concentrations and temperatures is observed. Figure 19 shows an example of the temperature evolution along the stagnation streamline of a hemispherical model. It is obvious that vibrational non-equilibrium effects in the flow around the body are strongly reduced because of the freezing of these quantities at a rather high level in the free stream of the nozzle. The same holds, of course, for the evolution of the species concentrations.

The shock detachment distances are found from the numerical simulations, and a comparison with corresponding values determined by interferometry is given in table 2. The agreement is fair since the discrepancies are about 2 % to 5 % which corresponds to the experimental uncertainties. The maximum discrepancy is observed for the largest sphere radius (50 mm). In this case, interactions between the detached bow shock and the boundary layer caused by the nozzle flow might be of importance. Effects of the expanding flow caused by the conical nozzle shape could also be of importance, but at high Mach numbers in a quasi-frozen flow, as for the present case, these effects have negligible influence on the shock stand-off distance (Hayes & Probstein 1959).

Finally, comparing the present values to those for the frozen case, a difference of only about 10 % is observed and the shock stand-off distance does not significantly

R [mm]	Δ/R (frozen)	Δ/R (non-equilibrium)	Δ/R (measured)
Condition 1:			
25	0.139	0.131	0.129
50	0.139	0.125	0.121
Condition 2:			
12.5	0.138	0.130	0.136
25	0.138	0.127	0.130
50	0.138	0.124	0.120

TABLE 2. Shock stand-off distances from numerical simulations and Hashimoto's experimental data.

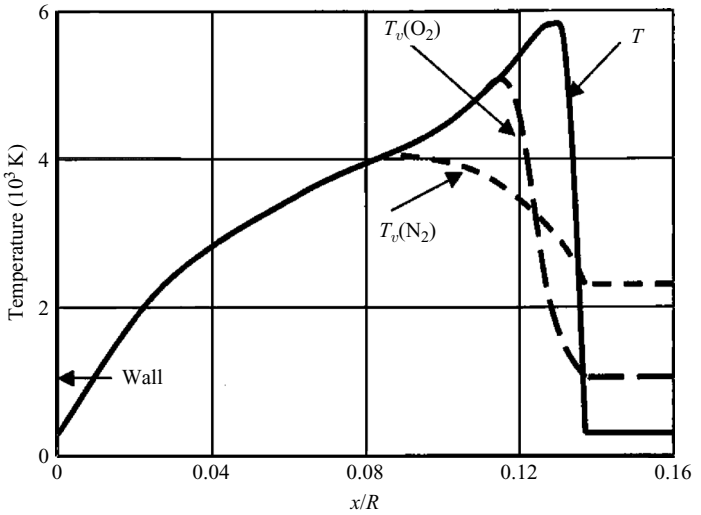

FIGURE 19. Temperature profiles along the stagnation line, Condition 1.

depend on the chemical conditions characterized by the flow conditions 1 and 2. This is also caused by the high Mach number and the quasi-frozen free stream. On the other hand, as for the case of the ballistic range, the two-temperature model (Park 1989*a*, *b*) underestimates the shock stand-off distance by about 10 % which is more than the uncertainty in the measurements and in the present computations which amounts to 5 %.

7. Conclusions

A theoretical model based on a quasi one-dimensional approach has been presented which allows determination of the shock stand-off distance on spheres and cylinders. A unique solution is obtained for the whole reactive flow regime ranging from frozen to equilibrium conditions. In spite of the use of the simple ideal dissociating gas model, it reveals the governing physical mechanisms of the hypersonic stagnation flow on blunt bodies. In a systematic manner it allows the study of the influence of the most important parameters on the shock stand-off distance, such as the density ratio between shock and body, the reaction rate parameter, the free-stream dissociation level, etc. A highly detailed solution of the flow field is obtained by the physical–numerical method described in the second part of the paper. This method, based on

the Chapman–Enskog method, allows to consideration of complex gas mixtures in thermal and chemical non-equilibrium including coupling between thermal excitation and chemistry. Whereas the theoretical method of the first part describes the main dependences of the most important parameters, the numerical solution allows a detailed analysis of the whole flow field. The values of the shock stand-off distance on hemispherical bodies computed by the present physical–numerical method are close to the experimental values, within less than 5 % which roughly corresponds to the experimental uncertainties. The same holds for the comparison with the results of the theoretical approach, when similar assumptions are made for the physical model used in both methods, which provides a reciprocal validation of these methods.

REFERENCES

Belouaggadia, N. & Brun, R. 1998 Chemical rate constants in non-equilibrium flows. *J. Therm. Heat Transfer* **12**, 482–488.

Belouaggadia, N. & Brun, R. 2006 Statistical model for vibration-chemical reaction interaction: Extension to gas mixtures. *J. Therm. Heat Transfer* **20**, 148–150.

Brun, R., Villa, M. P. & Meolans, J. G. 1984 Generalised transport terms in vibrationally relaxing flows. In *Rarefied Gas Dynamics* (ed. M. Oguchi). pp. 593–599. University of Tokyo Press.

Brun, R. 1988 Transport properties in reactive gas flows. *AIAA Paper* 88-2655.

Brun, R. 1991 Transport phenomena in relaxing gas mixtures: Models and applications. In *Rarefied Gas Dynamics* (ed. A. E. Beylich). pp. 379–390. VCH, Weinheim.

Freeman, N. C. 1958 Non-equilibrium flow of an ideal dissociating gas. *J. Fluid Mech.* **4**, 407–425.

Furudate, M., Nonaka, S. & Sawada, K. 1999 Behavior of two-temperature model in intermediate hypersonic regime. *J. Therm. Heat Transfer* **13**, 424–430.

Garr, L. J. & Marrone, P. V. 1963 Inviscid, non-equilibrium flow behind bow and normal shock waves, part II. *Cornell Aeron. Lab. Rep.* QM-1626-A-12(II).

Hall, J. G., Eschenroeder, A. Q. & Marrone, P. V. 1962 Blunt-nose inviscid airflows with coupled non-equilibrium processes. *J. Aero Space Sci.* **29**, 1038–1051.

Hashimoto, T. 2003 Analytical and experimental study of hypersonic nozzle flows in free piston shock tunnel. PhD Thesis AOTD1606, Tohoku University, Japan.

Hayes, W. D. & Probstein, R. F. 1959 *Hypersonic Inviscid Flow*. Academic.

Hornung, H. G. 1972 Non-equilibrium dissociating nitrogen flow over spheres and circular cylinders. *J. Fluid Mech.* **53**, 149–176.

Kogan, M. N., Galkin, V. S. & Makashev, N. K. 1979 Generalised Chapman-Enskog method: Derivation of the non-equilibrium gasdynamics equations. In *Rarefied Gas Dynamics* (ed. R. Campargue). pp. 693–734. CEA Paris.

Lick, W. 1960 Inviscid flow of a reacting mixture of gases around a blunt body. *J. Fluid Mech.* **7**, 128–144.

Lin, S. C. & Shen, S. F. 1951 An analytical determination of the flow behind a symmetrical curved shock in a uniform stream. *NACA Tech. Note* 2506.

Lobb, R. K. 1964 Experimental measurement of shock detachment distance on spheres fired in air at hypervelocities. In *The High Temperature Aspects of Hypersonic Flow* (ed. W. C. Nelson). pp. 519–527. Pergamon.

MacCormack, R. W. & Baldwin, B. S. 1975 A numerical method for solving the Navier-Stokes equations with application to shock-boundary interactions. *AIAA Paper* 75-1.

MacCormack, R. W. & Candler, G. 1989 The solution of the Navier-Stokes equations by Gauss-Seidel line relaxation. *Computers Fluids* **17**, 135–155.

Mazoue, F., Chikhaoui, A. & Brun, R. 1994 Non-equilibrium species concentration behind a normal shock wave in CO_2. In *Aerothermochemistry of Spacecraft and Associated Hypersonic Flows*. Jouve, Paris.

Millikan, R. C. & White, D. R. 1969 Systematics of vibrational relaxation. *J. Chem. Phys.* **39**, 3209–3213.

Nonaka, S. 2000 Experimental and numerical study on hypersonic flows in ballistic range. *Dept. of Aeronautics and Space Engineering*, Tohoku University, Sendai, Japan.

Olivier, H. 2000 A theoretical model for the shock stand-off distance in frozen and equilibrium flow. *J. Fluid Mech.* **413**, 345–353.

Park, C. 1985 On convergence of computation of chemically reacting flows. *AIAA Paper* 85-0247.

Park, C. 1989a A review of reaction rates in high temperature air. *AIAA Paper* 89-1740.

Park, C. 1989b Assessment of two temperature kinetic model for ionizing air. *J. Therm. Heat Transfer* **3**, 233–244.

Park, C. 1990 Review of finite-rate chemistry models for air dissociation and ionisation. In *Molecular Physics and Hypersonic Flows* (ed. M. Capitelli). pp. 581–596. NATO-ASI Series, Kluwer.

Pascal, S. & Brun, R. 1993 Tranport properties in non-equilibrium gas mixtures. *Phys. Rev.* **44**, 3251–3267.

Stupochenko, Y. V., Losev, S. A. & Osipov, A. I. 1967 *Relaxation in Shock Waves*. Springer.

Treanor, C. E. & Marrone, P. V. 1962 Effect of dissociation on the rate of vibrational relaxation. *Phys. Fluids* **5**, 1022–1027.

Van Dyke, M. D. 1958 The supersonic blunt body problem - review and extension. *J. Aero Space Sci.* **25**, 485–496.

Wen, C. Y. & Hornung, H. G. 1995 Non-equilibrium dissociating flow over spheres. *J. Fluid Mech.* **299**, 389–405.

Zlotnick, M. & Newman, D. J. 1957 Theoretical calculation of the flow on blunt-nosed axisymmetric bodies in a hypersonic stream. *Avco Mfg. Corp. Lawrence, MA, Tech. Rep.* 2-57-29.